ADVANCED HEALTHCARE MATERIALS
www.advhealthmat.de

Magnesium Oxide/Poly(L-lactide-co-ϵ-caprolactone) Scaffolds Loaded with Neural Morphogens Promote Spinal Cord Repair through Targeting the Calcium Influx and Neuronal Differentiation of Neural Stem Cells

Jile Xie, Jiaying Li, Jinjin Ma, Meimei Li, Xingran Wang, Xinya Fu, Yanxia Ma, Huilin Yang, Bin Li, and Saijilafu**

Because of the limited regenerative ability of the central nervous system (CNS), effective treatments for spinal cord injury (SCI) are still lacking. After SCI, neuron loss and axon regeneration failure often result in irreversible functional impairment. The calcium overload induced by the N-methyl-D-aspartate receptor (NMDAR) overactivation is critical for cell death in SCI. It has been reported that the magnesium ion (Mg^{2+}) can competitively block the NMDAR and reduce the calcium influx, and that sonic hedgehog (Shh) and retinoic acid (RA) are the critical regulators of neuronal differentiation of endogenous neural stem cells (NSCs). Here, magnesium oxide (MgO)/poly (L-lactide-co-ϵ-caprolactone) (PLCL) scaffold loaded with purmorphamine (PUR, a Shh signaling agonist) and RA is developed and its feasibility in SCI repair is tested. The results showed that the Mg^{2+} released from MgO attenuated cell apoptosis by blocking the calcium influx, and the PUR/RA promoted the recruitment and neuronal differentiation of endogenous NSCs, thereby reducing the glial scar formation at the SCI lesion site. Furthermore, implantation of PUR/RA-loaded MgO/PLCL scaffold facilitates the partial recovery of a locomotor function of SCI mouse in vivo. Together, findings from this study imply that PUR/RA-loaded MgO/PLCL scaffold may be a promising biomaterial for the clinical treatment of SCI.

1. Introduction

Spinal cord injury (SCI) often leads to partial or complete loss of sensory, motor, and autonomic functions below the lesion site, which seriously affects the patient's quality of life and brings a substantial medical burden on the patient's family and society. It is estimated that about 27 million people live with disabilities because of SCI, and there are as many as 0.92 million new cases each year worldwide.[1] Because of the limited regenerative ability of the central nervous system (CNS), most injuries are permanent, and effective treatments for SCI are still lacking. According to clinical guidelines, methylprednisolone is currently the only available drug for treating SCI; however, it has an ambiguous efficacy, strict dosing time, and a high risk for inducing complications.[2]

Because of the blood-spinal cord barrier and the complex pathophysiological process after SCI, it is not easy to achieve ideal efficacy in treating SCI with drugs or pharmacological agents. However, advances in biomaterial engineering techniques have brought a considerable promise for SCI treatment. After SCI, the primary injury leads to a series of cascade events, including excitatory amino acid release, cellular ion imbalance, cellular calcium overload, mitochondrial dysfunction, and immune and inflammatory responses. This further initiates a secondary injury cascade that aggravates the tissue damage, causes more cell death, and forms glial scars around the lesion site, which markedly hinders axon regeneration and growth.[3] Among these complex pathophysiological cascades, it is considered that the cell apoptosis caused by calcium overload is critical to the secondary injury in SCI. The overactivation of the N-methyl-D-aspartate receptor (NMDAR) induced by excitatory amino acids released from dead cells is key in mediating this process.[4] Therefore, blocking this step may interrupt the secondary injury loop of SCI and protect more neurons from apoptosis. It has been reported that the magnesium ion (Mg^{2+}) can competitively block NMDAR and voltage-gated calcium channels to reduce the calcium influx and

J. Xie, H. Yang, B. Li, Saijilafu
Department of Orthopaedics
The First Affiliated Hospital of Soochow University
899# Pinghai Road, Suzhou, Jiangsu 215006, China
E-mail: binli@suda.edu.cn; saijilafu@suda.edu.cn
J. Li, J. Ma, M. Li, X. Wang, X. Fu, Y. Ma, H. Yang, B. Li, Saijilafu
Orthopaedic Institute
Medical College
Soochow University
1# Shizi Road, Suzhou, Jiangsu 215006, China
The ORCID identification number(s) for the author(s) of this article can be found under https://doi.org/10.1002/adhm.202200386

DOI: 10.1002/adhm.202200386

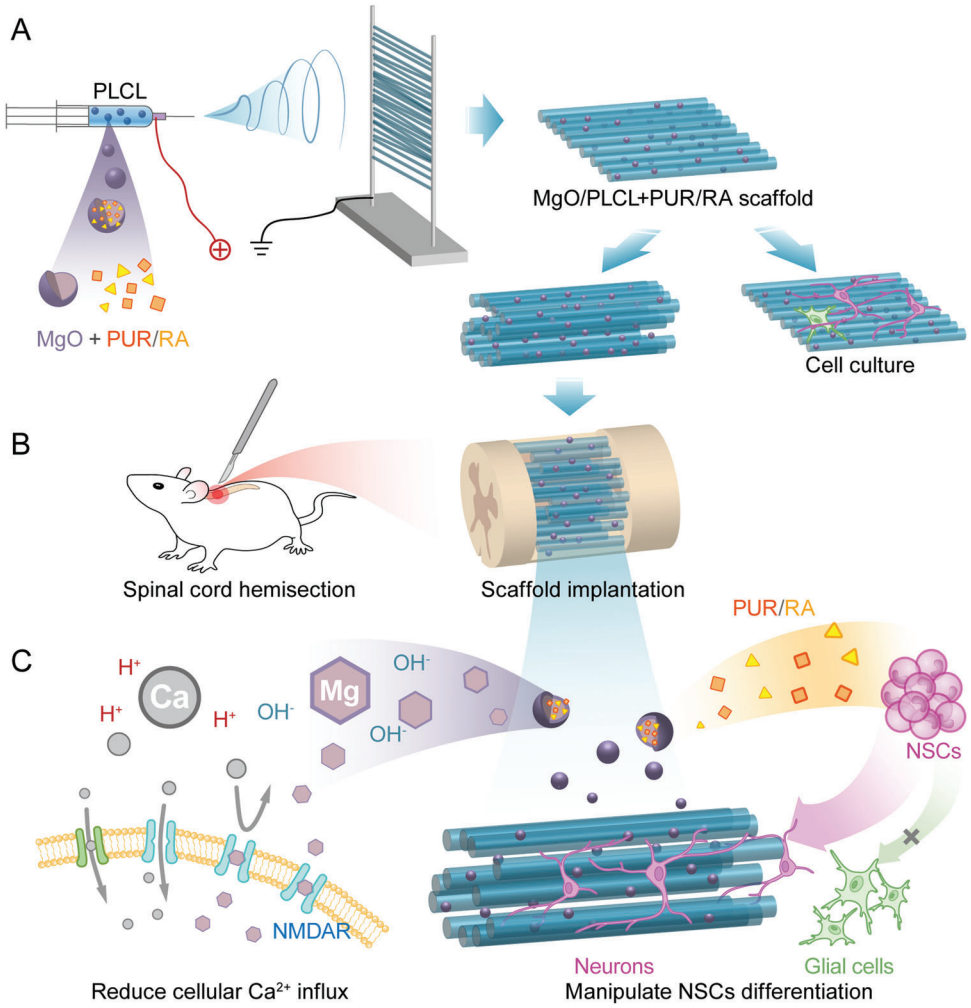

Figure 1. Schematic illustration of the study design. A) Demonstration of the fabrication of MgO/PLCL+PUR/RA scaffold with electrospun. B) The scaffold was implanted in mouse T9 spinal cord hemisection model. C) Demonstration of the mechanisms by which the scaffold works, the magnesium released from the scaffold blocks the cellular calcium influx by binding with NMDAR, and PUR and RA promote the neuronal differentiation of NSCs.

prevent calcium overload.[5] Magnesium has also been used for neuroprotection in the clinic, including eclampsia, preeclampsia, traumatic CNS injury, cerebral ischemia, stroke, and Parkinson's disease.[6] In addition, it was demonstrated that the decrease of Mg^{2+} after brain injury was directly linked to the deterioration of secondary injury.[7] Administration of magnesium within 8 h of SCI injury also showed the neuroprotective effect in an animal model.[8] Therefore, the local release of Mg^{2+} from the implanted biomaterials in SCI may be a more effective strategy to take advantage of because of the associated neuroprotective effect.

Studies have shown that some subsets of ependymal cells in the central canal of the spinal cord can be activated after SCI, acquiring the proliferation, migration, and differentiation abilities of neural stem cells (NSCs).[9] These endogenous NSCs are potentially powerful tools for reconstructing functional neural connections. However, most NSCs tend to differentiate into glial cells in the pathophysiological condition of SCI, which, together with the activated astrocytes, macrophages, and inhibitory extracellular matrix, form glial scars surrounding the lesion area.[10] At the early stage of SCI, the glial scars isolate the area of injury, preventing the spread of cytotoxic molecules and inflammatory factors to the adjacent area.[11] While in the chronic stage, these dense glial scars become barriers to axon outgrowth. Thus, inhibiting endogenous NSCs differentiation into glial cells is another valuable strategy for SCI repair. Sonic hedgehog (Shh) and retinoic acid (RA) are the critical regulators of neuronal differentiation in development and are also involved in endogenous self-repair after SCI.[12] However, the expression of Shh and RA is significantly declined in adults.[13] Thus, as biomaterial supplements, Shh and RA may be beneficial candidate factors for spinal cord regeneration.

Here, we prepared mesoporous magnesium oxide (MgO) nanoparticles to load purmorphamine (PUR, a Shh signaling agonist) and RA, followed by electrospinning with poly (L-lactide-co-ϵ-caprolactone) (PLCL) to fabricate aligned fibrous scaffolds (**Figure 1**A). PLCL is a biocompatible, degradable, and elastic polymer that has been reported to be a good candidate for tissue engineering.[14] The electrospun fibrous scaffold has high porosity and specific surface area, allowing nutrient exchange, cell penetration, and migration. At the same time, aligned scaffolds

prevent the regenerating axons from developing tortuous trajectories, instead directing their outgrowth along linear paths over the lesion site, facilitating functional connections with downstream targets. We found that MgO nanoparticles improved the biocompatibility of PLCL and exerted neuroprotective effects in acidic and NMDA-induced cytotoxic environments. Moreover, adding PUR and RA in MgO/PLCL promoted the neuronal differentiation of NSCs in vitro. More importantly, the implantation of PUR/RA-loaded MgO/PLCL scaffolds in a mouse spinal cord hemisection defect significantly promoted the recruitment of endogenous NSCs and their neural differentiation. At the same time, apoptotic cells around the scaffold were significantly reduced. Then, there was a marked decrease in glial scars and an increased number of neurons around the lesion site. In addition, these neurons sprout axons that grow along the orientation of the implanted scaffold, dramatically promoting motor function recovery.

2. Results

2.1. Characterizations of MgO Nanoparticles and MgO/PLCL Scaffolds

The porous MgO nanoparticles were synthesized via the complexation combustion method (**Figure 2**A). Transmission electron microscopy (TEM) imaging clearly showed the porous structure in MgO nanoparticles (Figure 2B), and elemental mapping confirmed the uniform distribution of metal species throughout the materials (Figure S1A, Supporting Information). The porous structure endows the MgO with adsorption capacity, which was further confirmed by the drug loading experiment. We found that the MgO could be loaded with 2.1% (w/w) PUR and 1.7% (w/w) RA simultaneously (Figure S1B, Supporting Information).

The scanning electron microscopy (SEM) imaging showed aligned fibers of MgO/PLCL scaffolds (Figure 2C). PLCL fibers were bead-free with a smooth surface. However, the MgO/PLCL fibers had spotted protrusions and rough surfaces (Figure 2C). The TEM imaging further confirmed that the MgO nanoparticles were incorporated in the PLCL fibers (Figure 2D). The fiber's diameter decreased with the increase in the MgO proportion. The diameters of MgO/PLCL fibers with a MgO:PLCL ratio of 0:100, 10:100, 25:100, and 50:100 were 1.30 ± 0.19 μm, 0.88 ± 0.15 μm, 0.94 ± 0.23 μm and 0.71 ± 0.17 μm, respectively, with a relatively uniform distribution (Figure 2E,F).

Further, tensile tests were performed to check the effect of MgO content on the mechanical properties of MgO/PLCL scaffolds (Figure 2G). The stress-strain curves in Figure 2H show that the tensile strength and modulus of scaffolds increased with MgO/PLCL ratio. The tensile modulus of MgO/PLCL at 0:100, 10:100, 25:100, and 50:100 ratios were 1.37 ± 0.17 MPa, 5.46 ± 0.95 MPa, 13.75 ± 1.17 MPa, and 16.20 ± 1.16 MPa, respectively (Figure 2I).

The MgO nanoparticles incorporated in PLCL improved the hydrophilicity of the scaffolds. The water contact angle was $113.40 \pm 3.78°$ for the PLCL scaffold, and $95.28 \pm 12.05°$, $78.48 \pm 4.61°$, and $68.62 \pm 4.21°$ for the MgO/PLCL scaffolds with a ratio of 10:100, 25:100 and 50:100, respectively (Figure 2J).

The Mg^{2+} release profile was detected using a commercial kit, and the MgO/PLCL scaffolds of all three ratios showed similar initial burst release within 1 h (Figure 2K). The Mg^{2+} concentration of the MgO/PLCL (50:100 and 25:100) increased smoothly and reached a saturation concentration of 2.34 ± 0.07 mM at 2 weeks. In contrast, MgO/PLCL (10:100) scaffold released Mg^{2+} more slowly and did not reach saturation even after 4 weeks (Figure 2K). The dissolution profile of the MgO/PLCL (25:100) scaffold showed that 8.87% (w/w) of MgO was dissolved after 4 weeks, at a relatively uniform rate, reflecting its degradation characteristic (Figure 2L).

2.2. Biocompatibility of MgO/PLCL Scaffolds in Vitro

The scaffolds were seeded with bone marrow mesenchymal stromal cells (BMSCs) to evaluate their biocompatibility. The BMSCs adhered to the scaffolds in each group and extended along the fiber direction (**Figure 3**A). Because of the hydrophobicity, the spreading area of BMSCs on PLCL was less than the control group. However, the spreading area increased slightly by adding MgO until the ratio reached 50:100. Quantitative analysis showed that the spreading area of BMSCs on MgO/PLCL (25:100) scaffolds was better than the other groups (Figure 3B). It is reasonable to infer that the MgO changed the morphology of PLCL fibers and improved its hydrophilicity, which was conducive to the adhesion and spreading of cells. Too much MgO (50:100) seemed to excessively reduce the fiber diameter, which hindered the lateral spread of cells. Thus, considering the physical properties and cell adhesion, a MgO/PLCL ratio of 25:100 was adopted in our subsequent experiments.

2.3. MgO/PLCL Scaffolds Protected Neurons in the Acidic Environment

The culture medium (pH 6.5) was neutralized to pH 7.35 upon contact with MgO/PLCL (25:100) scaffolds for as short as 3 min, and then the rise in pH value reached a plateau and stabilized at weak alkaline (Figure 3C,D). This is in accordance with the nature of MgO as a strong electrolyte that is very slightly dissoluble in water. From this, we can infer that MgO endowed the PLCL scaffold with the ability to rapidly neutralize acids in the environment. Further, we verified the effect of the MgO/PLCL scaffold on neuronal protection via live/dead cell staining (Figure 3E). The culture medium of pH 6.5 was used to mimic the acidic environment after SCI.[15] After culturing in the pH 6.5 medium for 48 h, the survival rate of cortical neurons decreased from $61.96 \pm 3.45\%$ to $42.35 \pm 2.57\%$ ($p = 0.0092$), with similar results in PLCL group ($66.68 \pm 11.38\%$ to $43.93 \pm 2.66\%$, $p = 0.0027$) (Figure 3F). However, the addition of MgO to scaffolds significantly improves neuronal survival in acidic environments, and the cell viability was not statistically different from that in the normal medium ($p = 0.91$ in MgO/PLCL group) (Figure 3F).

2.4. MgO/PLCL Scaffolds Suppressed NMDA-Induced Cell Apoptosis

We used N-methyl-D-aspartate (NMDA, 50 μM), a specific agonist of NMDAR, to simulate the excitotoxic environment caused by glutamate-induced cellular Ca^{2+} influx after SCI.[16] The

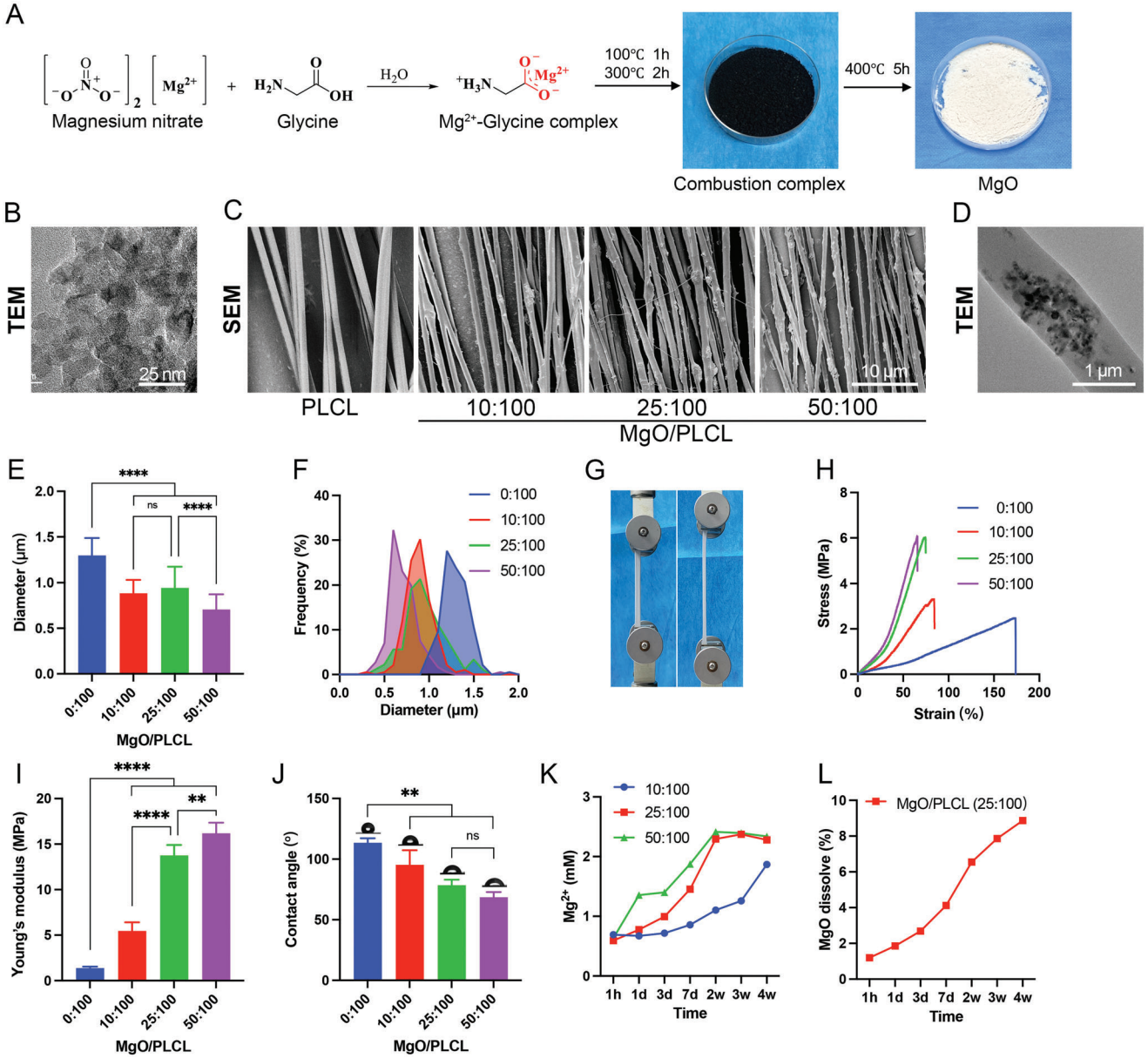

Figure 2. Characterization of MgO/PLCL scaffolds. A) Schematic illustration of the synthesis of mesoporous MgO nanoparticles. B) TEM image of synthesized mesoporous MgO nanoparticles. C) SEM images of MgO/PLCL scaffolds with different proportions of MgO nanoparticles. D) TEM image of MgO/PLCL (25:100) fiber. E) Diameter comparison of MgO/PLCL fibers. F) Diameter frequency distribution of MgO/PLCL fibers. G) Tensile test of scaffolds. H) Tensile stress-strain curve of scaffolds. I) Young's modulus of scaffolds. J) Water contact angle test of scaffolds. K) Mg^{2+} release property of scaffolds with different ratios. L) MgO degradation profile of MgO/PLCL (25:100). $^{**}p < 0.01$, $^{****}p < 0.0001$.

Fluo-4 AM validated the increased neuronal Ca^{2+} influx induced by NMDA (**Figure 4**A,B). After being treated with NMDA for 24 h, cortical neurons showed 30.66 ± 7.15% apoptosis in the control group and 28.57 ± 8.87% cell apoptosis in the PLCL group. In contrast, the proportion of apoptotic cells was 8.16 ± 2.27% in MgO/PLCL group, significantly lower than control and PLCL groups ($p < 0.05$ for both) (Figure 4C,D). Therefore, because NMDA can induce the Ca^{2+} influx, thus it can be inferred that the MgO in scaffolds reduced the NMDA-induced cell apoptosis via blocking Ca^{2+} influx.

2.5. PUR/RA-Loaded MgO/PLCL Scaffolds Promoted Neuronal Differentiation of NSCs and Axons Extension in Vitro

The NSCs of E14 fetal mice were isolated and cultured to examine the effect of scaffolds on their differentiation potential (Figure S2, Supporting Information). The cell differentiation was identified via neuron marker β-Tubulin (Tuj1) and the astrocyte marker glial fibrillary acidic protein (GFAP) after coculturing with scaffolds for 7 days (**Figure 5**A). Our results showed that NSCs tended to differentiate into astrocytes rather than neurons in control,

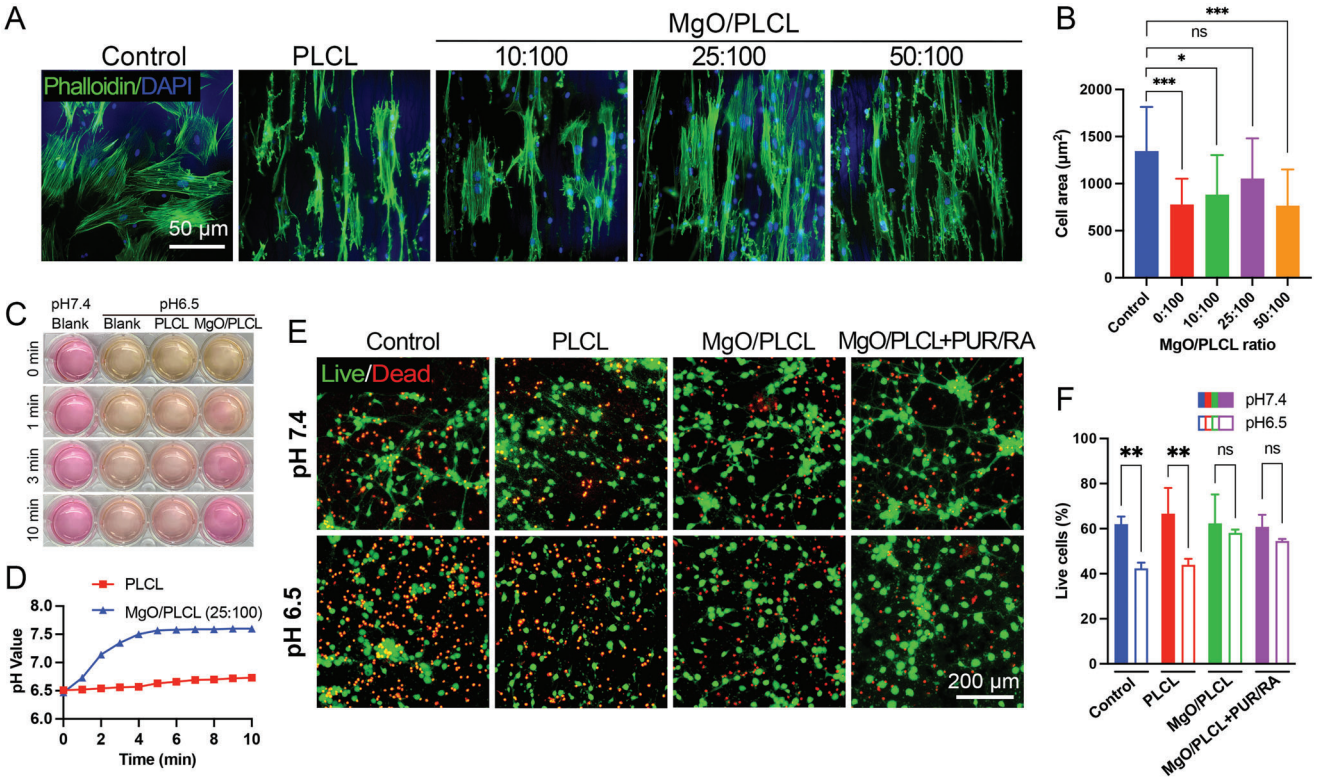

Figure 3. Cytocompatibility tests of MgO/PLCL scaffolds. A) Cytoskeleton staining of BMSCs seeded on MgO/PLCL scaffolds with different ratios. B) Quantification of cell area of BMSCs seeded on scaffolds. C-D) pH response of MgO/PLCL (25:100) in acidic environment. E) Live/dead cell staining of cortical neurons co-cultured with scaffolds in normal and acidic culture medium. F) Quantification of live/dead cell staining. $*p < 0.05$, $**p < 0.01$, $***p < 0.001$.

PLCL, and MgO/PLCL groups. The percentage of neurons in each group was 5.66 ± 1.42%, 6.10 ± 3.11%, 6.83 ± 2.88%, respectively ($p > 0.05$ compared with each other). While loading PUR/RA on the MgO/PLCL scaffold, the proportion of astrocytes was markedly reduced, and the number of neurons significantly increased (14.18 ± 1.61%, compared with the other three groups, $p = 0.0099$, $p = 0.0133$, $p = 0.0220$, respectively) (Figure 5E). The results indicated that PUR/RA enhanced the differentiation of NSCs into neurons, which is more beneficial for nerve repair. The morphological characteristics of axons of differentiated neurons were evaluated using a concentric circle (Sholl's) analysis. We found that beyond 140 μm away from the soma, the density of neurites on MgO/PLCL and PUR/RA-loaded MgO/PLCL scaffolds was higher than that of the control group, reflecting the guidance of scaffolds on axons (both $p < 0.05$) (Figure 5D). The farthest linear distance of axon extension on the PUR/RA-loaded MgO/PLCL scaffold was up to 380 μm, much higher than that of 260 μm in the control group (Figure 5D). Moreover, we noted that the axons sprouting from a particular neuron extended along the scaffold for a surprising length, demonstrating the favorable support of the scaffold on axonal extension (Figure 5B). In addition, since the Nestin-labeled intermediate filament are involved in the migration of cells, the aligned distribution of Nestin suggested that the scaffolds guided the migration of NSCs (Figure 5C). The EdU staining and CCK-8 assay demonstrated that the proliferation rate and viability of NSCs were not affected by the addition of MgO or the loading of PUR/RA on the scaffolds (Figure 5F,G).

2.6. PUR/RA-Loaded MgO/PLCL Scaffolds Promoted Spinal Cord Repair in Vivo

2.6.1. PUR/RA-Loaded MgO/PLCL Scaffolds Recruited Endogenous NSCs to the Lesion Site

The PLCL and PUR/RA-loaded MgO/PLCL scaffolds were implanted into a hemisection defect injury at the T9 level of the adult mouse spinal cord (**Figure 6**A). Two weeks later, endogenous NSCs recruitment was found by immunostaining of Nestin, a well-known marker of NSCs. The presence of Nestin$^+$ cells around the lesion site indicated the activation of endogenous NSCs. Unfortunately, the endogenous NSCs stumped at the edge of the lesion site in the control group had no scaffold implantation (Figure 6C). In contrast, activated NSCs gathered around the scaffolds in both PLCL and PUR/RA-loaded MgO/PLCL groups (Figure 6C). Moreover, the endogenous NSCs were much more activated in the central canal of the spinal cord in PUR/RA-loaded MgO/PLCL group compared with the other two groups. A Nestin$^+$ cell migrating path from the spinal cord central canal to

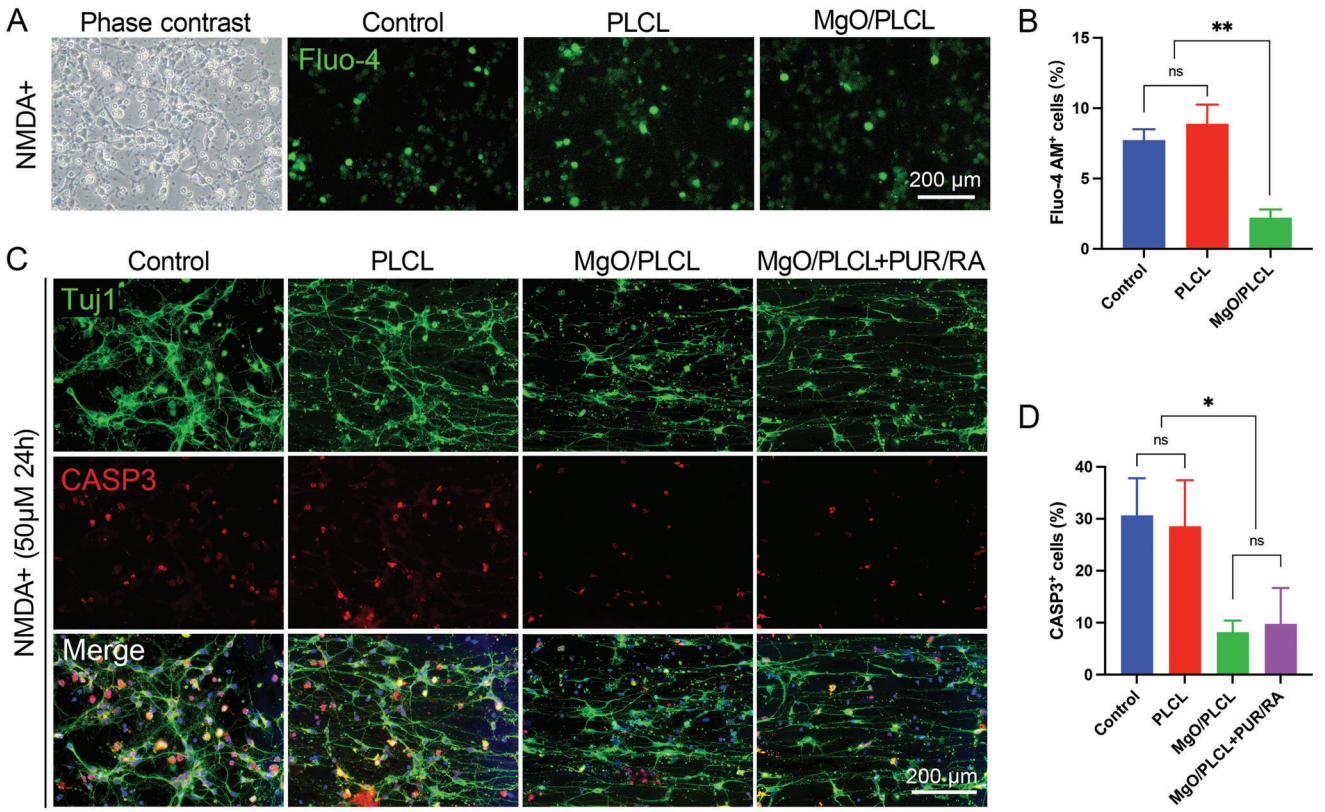

Figure 4. Neuroprotective effect of MgO/PLCL scaffold in vitro. A) Cellular calcium imaging by Fluo-4 AM. B) Quantification of Fluo-4 AM$^+$ cells. C) Immunofluorescence (IF) imaging of NMDA-induced cell apoptosis marked by CASP3. D) Quantification of CASP$^+$ cells in each group. *$p < 0.05$, **$p < 0.01$.

the implanted scaffold was observed, revealing that the PUR/RA promotes the migration of endogenous NSCs to the scaffolds (Figure 6C).

2.6.2. The Neuroprotective Effect of PUR/RA-Loaded MgO/PLCL Scaffolds at the SCI

Our in vitro experiments have confirmed that the MgO in scaffolds has a protective effect on cell apoptosis via blocking calcium influx. Thus, we attempted to further confirm this effect in vivo. Two weeks after SCI, the apoptotic cells (labeled by CASP3) were observed around the lesion site in the control group (33.75 ± 7.68 cells per visual field) and the PLCL group (26.00 ± 5.77 cells per visual field). In comparison, the number of CASP3$^+$ cells around the PUR/RA-loaded MgO/PLCL scaffolds (11.25 ± 5.74 cells per visual field) was significantly reduced compared with the other two groups ($p = 0.0021$, $p = 0.0253$, respectively; Figure 6D,E). This suggests that the Mg^{2+} released from the scaffolds also prevents neuronal death in vivo. In addition, we also observed more mature neurons labeled by NeuN around the PUR/RA-loaded MgO/PLCL scaffolds compared with the other two groups, indicating the improved survival of neurons (Figure 6D).

One concern about MgO implantation is the influence of its alkalinity on the local environment. To address this issue, we quantified the RNA expression of the acid-sensing ion channel 3 (ASIC3) gene and alkaline sensing channel (PKD2L1) gene of the spinal cord via real-time polymerase chain reaction (RT-PCR) during the acute period (3 days) and chronic period (4 weeks) after SCI. The results showed that the expression of the ASIC3 gene in the PLCL group was upregulated in both the early and late stages after SCI, while the group with MgO incorporated had no significant difference from the control group (Figure 6F). From this finding, we inferred that the presence of MgO counteracted the effect of acid products generated by PLCL degradation in the spinal cord. The expression of PKD2L1 was upregulated in the PUR/RA-loaded MgO/PLCL group 3 days after SCI and decreased to a normal level 4 weeks later, suggesting that the alkaline products of MgO degradation affected the spinal cord at an early stage, but this effect was temporal (Figure 6F).

2.6.3. PUR/RA-Loaded MgO/PLCL Scaffolds Reduced Glial Scar Formation and Promoted Axon Regeneration

To examine the effect of PUR/RA-loaded MgO/PLCL scaffolds on endogenous NSCs differentiation, Tuj1 and GFAP immunostaining were conducted at 8 weeks after implantation surgery. In the control group, massive astrocytic glial scars (GFAP) formed hypertrophic processes that densely overlap and pack around the lesion area, and only a few scattered, disordered axons were observed at the epicenter of the lesion (**Figure 7**A).

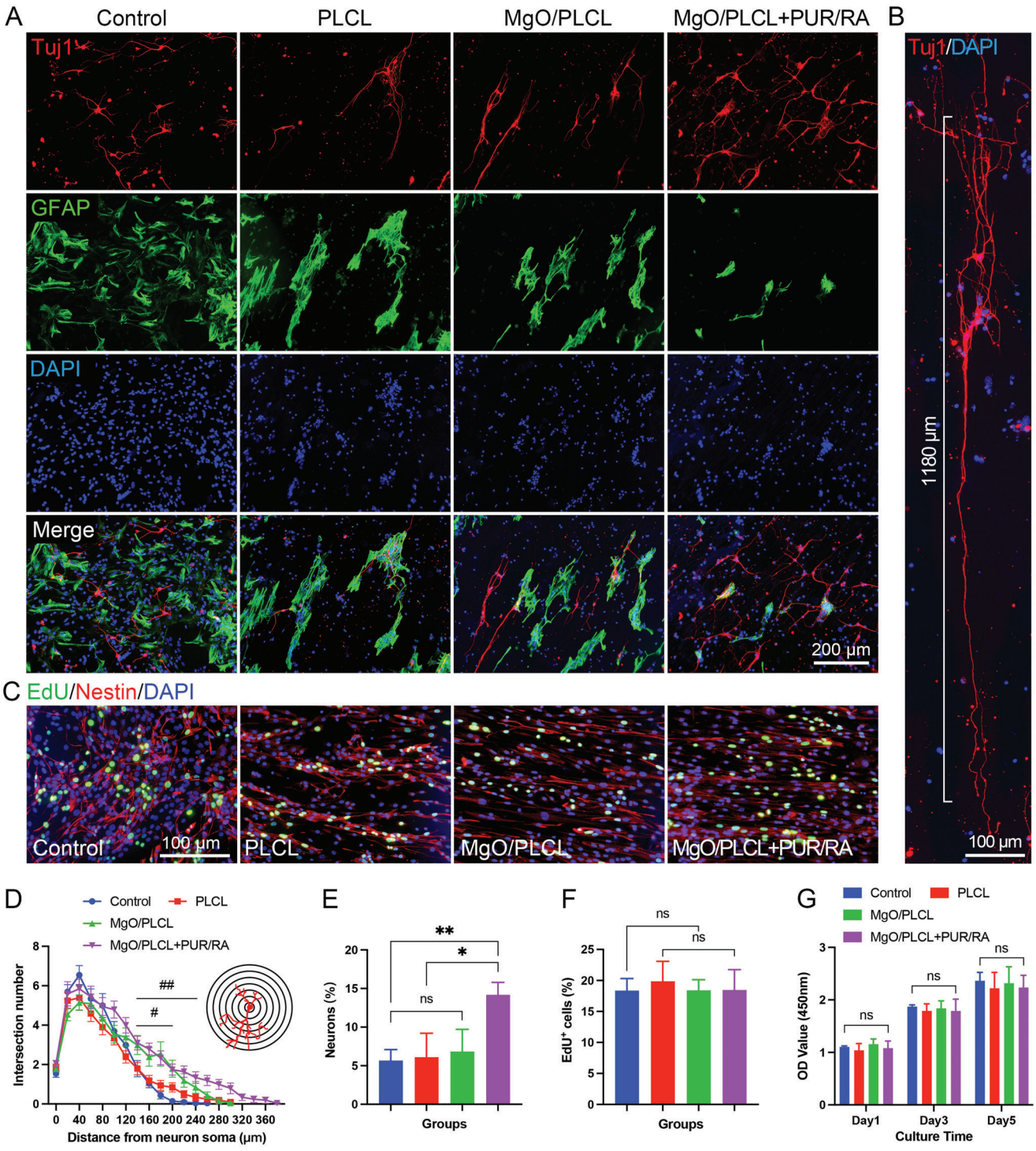

Figure 5. NSCs differentiation assay on scaffolds. A) IF staining of NSCs differentiation on scaffolds. B) Axons grow along the MgO/PLCL+PUR/RA scaffold with a long distance. C) NSCs proliferation labeled by EdU and Nestin on scaffolds. D) Sholl's analysis of axons of neurons differentiated from NSCs ($^{\#}$MgO/PLCL versus control, $p < 0.05$, $^{\#\#}$MgO/PLCL+PUR/RA versus control, $p < 0.05$). E) Quantification of neurons differentiated from NSCs on scaffolds. F) Quantification of EdU^{+} cells in Figure 5C. G) NSCs proliferation assay via CCK-8. *$p < 0.05$, **$p < 0.01$.

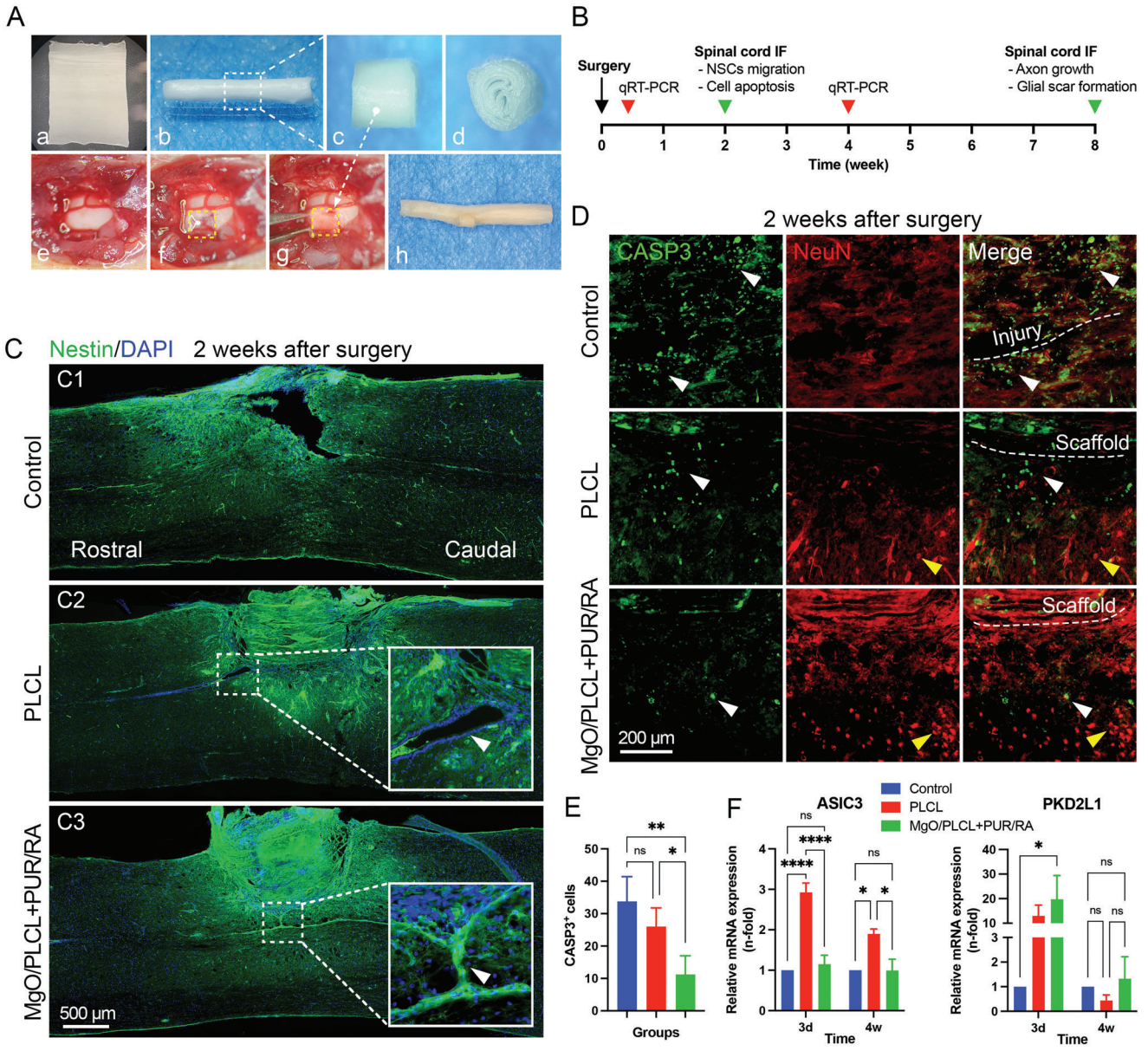

Figure 6. Evaluations on the NSCs recruitment and neuroprotective effect of MgO/PLCL+PUR/RA scaffold in vivo. A) Preparation (a-d) and implantation (e-g) of the scaffold, (h) integration of scaffold with spinal cord. B) Schematic diagram of the in vivo experiments. C) IF staining of the recruitment of NSCs marked by Nestin at 2 weeks after surgery. D) IF staining of CASP3-labeled apoptotic cells (white arrowhead) and NeuN-labeled survival neurons (yellow arrowhead) at 2 weeks after surgery. E) Quantification of CASP3$^+$ cells around the injury site. F) RT-PCR study of ASIC3 gene and PKD2L1 gene of the spinal cord at 3 days and 4 weeks after the surgery. *$p < 0.05$, **$p < 0.01$, ****$p < 0.0001$.

In contrast, the GFAP$^+$ area was mild and restricted in the PLCL and MgO/PLCL+PUR/RA scaffolds, indicating a suppressed astrocytosis (Figure 7A,B). In addition, scattered GFAP was observed to penetrate PLCL scaffolds but not MgO/PLCL+PUR/RA scaffolds (Figure 7A). The Tuj1-labeled neurons were observed in both scaffolds, corroborating the recruitment of endogenous NSCs to scaffolds at an early period (Figure 7A, Figure S3, Supporting Information). Interestingly, it is evident that numerous neuronal clusters were observed inside the edge of the PUR/RA-loaded MgO/PLCL scaffolds, which sprouted axons with long-distance growth (Figure 7g, Figure S3, Supporting Information). Given that the mature neurons lacked migration ability, it is reasonable to infer that the PUR and RA may promote the neuronal differentiation of recruited NSCs. We further examined the chondroitin sulfate proteoglycans (CSPG) and microglia cells (CD68) and found that similar to GFAP, CSPG was restricted around the scaffolds and CD68$^+$ microglia cells in MgO/PLCL+PUR/RA group were less than the other two groups (Figure S4, Supporting Information).

The motor function recovery of the hind limb was evaluated weekly via the Basso Mouse Scale (BMS) score after surgery ($n = 10$). The typical locomotion defect after SCI in mice is the dorsal

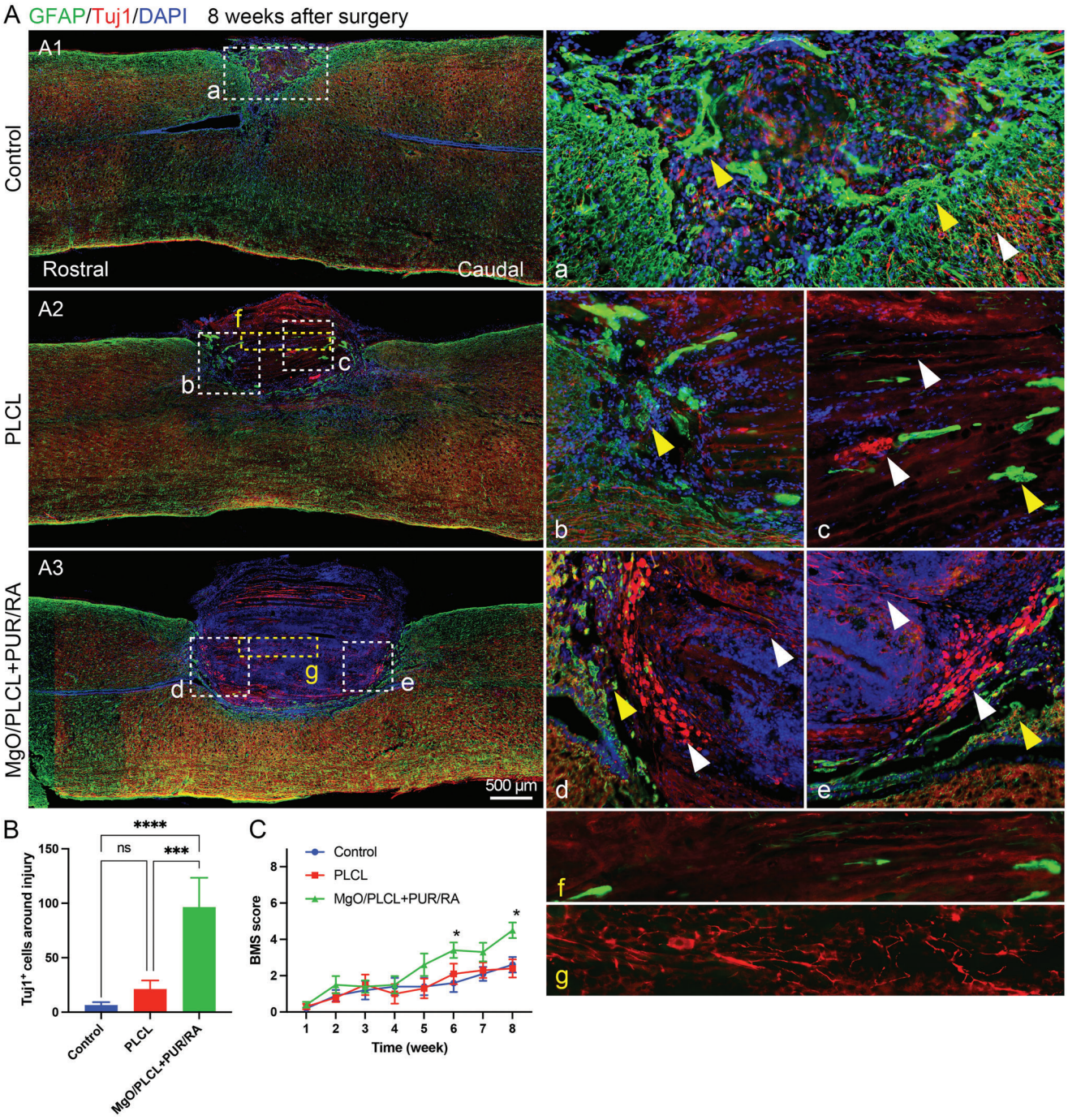

Figure 7. Nerve repair of MgO/PLCL+PUR/RA scaffold in vivo. A) GFAP-labeled glial formation (yellow arrowhead) and Tuj1-labeled neuronal differentiation (white arrowhead) around the injury site and scaffolds at 8 weeks after surgery. B) Quantification of neurons in each group. C) Locomotion recovery assessment. *$p < 0.05$, ***$p < 0.001$, ****$p < 0.0001$.

placing of paws without active motion. Here, 4 points of the BMS score represent plantar stepping, which indicates the recovery of leg muscles. The locomotion recovered slightly in both the control and PLCL groups; however, it did not reach 4 points during the 8-weeks follow-up. Surprisingly, compared with the PLCL group, PUR/RA-loaded MgO/PLCL implantation showed a better functional recovery with statistical differences at 6 weeks after surgery ($p = 0.042$). The BMS score reached 4.2 ± 1.3 points at 8 weeks after surgery, significantly higher than the other two groups ($p = 0.048$ and 0.012, compared with the control and PLCL group, respectively) (Figure 7C). These results indicate that the implantation of PUR/RA incorporated MgO/PLCL scaffolds significantly promoted the locomotion recovery of SCI.

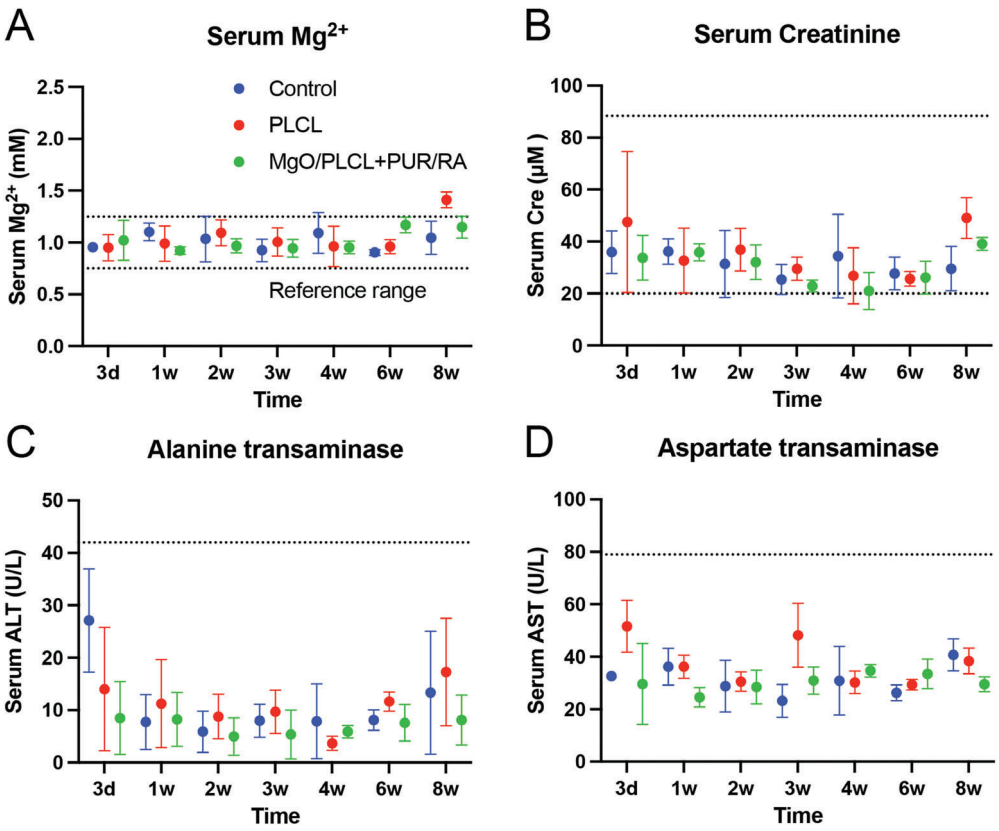

Figure 8. Biosafety of scaffolds in vivo. A) Serum Mg^{2+} concentration. B) Serum creatinine concentration. C) Serum alanine transaminase activity. D) Serum aspartate transaminase activity.

2.7. Biocompatibility of Scaffolds in Vivo

The continuous release of Mg^{2+} from MgO-incorporated scaffolds raises concerns about its long-term in vivo biosafety. Therefore, the serum Mg^{2+} level and blood biochemical indicators were measured weekly after implantation surgery. The serum Mg^{2+} concentration in each group was maintained in the normal range during the follow-up, indicating that PUR/RA-loaded MgO/PLCL scaffolds did not induce a higher blood Mg^{2+} concentration (**Figure 8**A). In addition, the serum creatinine (Cre), alanine transaminase (ALT) activity, and aspartate transaminase (AST) activity were all within the normal range during the follow-up, suggesting that the Mg^{2+} release from the scaffolds did not impair renal and liver function and were safe for in vivo implantation (Figure 8B,C,D).

3. Discussion

The pathophysiological processes involved in SCI include a primary injury and a subsequent cascade of insults. The primary injury is irreversible, but the secondary injury cascade is theoretically treatable, although it persists for a long time and results in morbidity.[17] Emerging evidence suggests that magnesium could ameliorate traumatic brain injury.[6c] Additionally, magnesium can support neuronal survival after traumatic brain injury through various mechanisms, including inhibition of presynaptic excitatory neurotransmitter release, blocking of NMDA channels and voltage-gated calcium channels, and potentiation of presynaptic adenosine.[18] Both laboratory and clinical studies have documented that serum Mg^{2+} is decreased after traumatic brain injury, and this Mg^{2+} decrease is associated with the development of neurological dysfunction.[7,19] In addition, its neuroprotective effects were only demonstrated following high doses of Mg^{2+}, and lower doses were less effective in providing significant physiological or functional benefits.[20] However, the Mg^{2+} transport capacity of the blood-spinal fluid-barrier is limited; high-dose intravenous Mg^{2+} administration only leads to a modest increase (16%–18%) of Mg^{2+} in cerebrospinal fluid.[21] Several studies applied Mg^{2+} intravenously for traumatic brain injury but yielded conflicting results.[18,22] Given this condition, some studies tried to combine Mg^{2+} with polyethylene glycol (PEG), a hydrophilic polymer used as an excipient for many drugs, to reduce the dosage needed and have achieved relatively positive results.[23]

This study developed a bioengineered scaffold for the topical release of Mg^{2+} in the spinal cord. MgO has been used as an antacid and magnesium supplement in the clinic and incorporated into orthopedic materials to promote osteogenesis.[24] The properties of MgO make it a favorable candidate as a source of Mg^{2+} in vivo. First, MgO is slightly soluble in water (0.009%, PubChem CID 14 792) and reaches saturation at an Mg^{2+} concentration of 2.1 mM, which is close to the therapeutic serum Mg^{2+} concentration.[20] Second, the dissolved MgO forms $Mg(OH)_2$, a strong electrolyte that may quickly neutralize the SCI-induced

acidic microenvironment without over-alkalinization. These features of MgO were preserved in MgO/PLCL fibers, and they conferred the scaffolds with an appropriate response in an acidic environment and mild Mg^{2+} release properties in the liquid environment. In this study, the MgO/PLCL scaffold properties were also compatible with neural cell survival and proliferation in vitro. In addition, the combustion method enhanced porosity to MgO, giving it the adsorption capacity to load drugs. Since both PUR and RA are insoluble in water, the release properties of drugs could not be modeled in the liquid environment; however, the degradation rate of MgO could indirectly reflect the release rate of the drugs.

Different proportions of MgO in fibers modified the physical properties of MgO/PLCL scaffolds. Increasing the proportion of MgO would yield finer fibers, probably because the presence of MgO nanoparticles increased the electrical conductivity of the solution, which further increased the acceleration of the jet, resulting in decreased fiber diameters.[25] The MgO/PLCL (25:100) had diameters similar to that of MgO/PLCL (10:100) but a higher Young's modulus and ultimate tensile strength. We speculate that the MgO nanoparticles incorporated in the polymers resisted the elongation of fibers, resulting in a higher modulus. In addition, the presence of MgO nanoparticles increased the roughness of the fiber surface on the nanoscale, which improved the hydrophilicity and contributed to better cell adhesion compared with the pure PLCL scaffold. After assessing the properties of MgO/PLCL scaffolds with different proportions, we determined that a ratio of 25:100 for MgO/PLCL is a relatively reasonable candidate, as it combines good hydrophilicity and Mg^{2+} release characteristics. Various polymer-based scaffolds, including polylactic acid (PLA), poly (lactic-co-glycolic acid) (PLGA), and poly-ϵ-caprolactone (PCL), have been investigated for SCI repair. However, the degradation products were acidic and detrimental to nerve repair.[26] Fortunately, this problem could be solved by the MgO nanoparticles used in this study. The MgO nanoparticles modified the acidic microenvironment of SCI and neutralized the acidic products generated by polymer degradation.

One of the primary mechanisms by which Mg^{2+} performs neuroprotection is via its interaction with NMDAR. In the acute to the subacute period of SCI, ischemia and excitotoxicity lead to disturbances of intracellular and extracellular ionic homeostasis, with intracellular calcium dysregulation being a pivotal mediator of cell death.[27] High levels of glutamate are released from dying cells, causing NMDAR overactivation, which subsequently results in calcium influx, triggering mitochondrial dysfunction and excitotoxic cell death. The excitotoxic cell death, combined with ischemia and inflammation, cyclically propagates the secondary injury cascade.[17] Magnesium can bind to a specific site on NMDAR to block the calcium channel, reducing the accumulation of cytotoxic levels of intracellular calcium.[28] In this study, we simulated the increased cellular calcium influx by NMDAR overactivation in vitro and demonstrated the neuroprotective effect of Mg^{2+} released by scaffolds both in vitro and in vivo. The concentration of Mg^{2+} around the MgO/PLCL scaffold was approximately twice the physiological concentration, which was right in the optimal range for neuroprotection (2.0–2.5 mM).[20] Moreover, the Mg^{2+} released by the scaffold did not increase serum Mg^{2+}, and this could be explained by the stable and slow degradation rate of MgO and the limited ion transport capacity of the blood-spinal fluid barrier. This is important to reduce the burden on the kidneys because Mg^{2+} is mainly metabolized by these organs.

Recent studies have revealed that a subpopulation of spinal cord ependymal cells can be activated after SCI to possess neural stem cell properties.[9a] In this study, although activation and recruitment of NSCs were observed in all groups at 2 weeks after surgery, a higher proportion of Nestin-labeled NSCs was noted in the ependymal zone around PUR/RA-loaded MgO/PLCL scaffold. This is supposed to be the effects of RA and PUR. Pfenninger et al. reported that ependymal cells express several RA-regulated genes, and RA promoted the survival and proliferation of ependymal cells via binding to PPARβ/δ, which functions as a heterodimer with RXR.[29] Previous studies have shown that RA and Shh are involved in neuronal differentiation and the survival and proliferation of NSCs.[30] The absence of RA significantly reduces the survival of NSCs in vivo.[31] Considering the importance of NSCs in neural regeneration, the multiple biological functions of RA and PUR may provide additional advantages for repairing SCI.

The cell differentiation fate of NSCs was further tracked by immunofluorescence staining of the protein marker Tuj1 and GFAP. After SCI, studies have reported that endogenous NSCs tend to differentiate into astrocytes and oligodendrocytes.[10b] Our strategy for manipulating the differentiation was inspired by the natural developmental pattern of the spinal cord. Studies in the developing spinal cord have demonstrated that the varying levels of Shh secreted by the floor plate and notochord, and RA produced by somite, result in graded levels of the Gli transcription factors along the dorso-ventral axis of the neural tube, allowing the morphogen gradient to be translated into the transcriptional control of neuronal differentiation.[32] The ventral regions with higher Shh and RA concentrations form five ventral progenitor cell domains (p0, p1, p2, pMN, and p3) and eventually differentiate into neural cells, including motor neurons.[33] In this study, the neuron clusters around the scaffold incorporated with PUR and RA validated the effect of the functional scaffold in directing the neuronal differentiation of NSCs in vivo. These neurons sprout plenty of axons that grow along the scaffold with long distances and through the injury area, making it possible to reconstruct functional connections in long-range defects in SCI. More importantly, a small number of Tuj1-labeled neurons were observed in the middle of the scaffold, acting as neural relays for the axons. Furthermore, substantial axon growth was observed only in PUR/RA-loaded MgO/PLCL groups, suggesting that regulating the cellular environment and signaling pathways may play a more critical role in axon regeneration, while the scaffold structure alone is not sufficient to support nerve repair.

While most studies placed the promotion of neuronal and axonal regeneration as the primary target, we considered that promoting the survival of nerve cells is as crucial as nerve regeneration. This is because the spinal cord has automatic execution centers that produce stereotypical motor patterns that allow for complex movements without supraspinal inputs.[34] The survival of neurons around the lesion site implies an increased possibility of preserving spinal cord execution centers. Even minor axon regeneration across the injury area may result in meaningful improvements in functional recovery. Considering the complex pathophysiology and the poor intrinsic recovery potential of neurons after SCI, the strategy used in this study

may have a better cost-effectiveness ratio. Taken together, the primary goals of the PUR/RA-loaded MgO/PLCL scaffold designed in this study were to rescue neurons from the calcium influx and acidic microenvironment-induced death in SCI, to promote the neuronal differentiation of endogenous NSCs at the lesion site, and to promote the extension of regenerated axons along linear paths to bridge the injured spinal cord.

4. Conclusion

In this study, we have verified the efficacy and safety of topical application of magnesium in SCI repair. The MgO neutralized the acidic environment and released Mg^{2+} to inhibit nerve cell apoptosis by blocking Ca^{2+} influx. Subsequently, the loading of PUR and RA promoted the neuronal differentiation of endogenous NSCs and decreases glial cell differentiation. Finally, implantation of PUR/RA-loaded MgO/PLCL scaffolds into spinal cord defects significantly protected nerve cell death and inhibits glial scar formation around the SCI lesion site. Furthermore, implantation of PUR/RA-loaded MgO/PLCL scaffolds promoted partial locomotor functional recovery of the hind limb of the SCI mouse without renal and liver function impairment in vivo. Together, findings from this study have suggested that PUR/RA-loaded MgO/PLCL scaffolds might be promising transplantation material for treating SCI in clinics.

5. Experimental Section

Synthesis and Characterizations of MgO Nanoparticles: Mesoporous MgO nanoparticles were synthesized based on previous research.[35] Briefly, magnesium nitrate hexahydrate ($Mg(NO_3)_2.6H_2O$) (99%, LingFeng, China) and fuel glycine (99%, BioFroxx, China) at a mass ratio of 1:1.5 were completely dissolved in distilled water. This mixture was heated to evaporate the water and obtain wet powder, and then the heating was continued up to 300 °C for 1 h to dehydrate and obtain a combusted metal precursor. The metal precursor was then calcined at 400 °C for 5 h to obtain a white porous foamy substance (mesoporous MgO nanoparticles). The microstructure of MgO nanoparticles was observed via transmission electron microscopy (TEM) (Hitachi, HT7700, Japan) with elemental mappings.

All the drug loading performances were carried out under yellow light. The procedure was carried out by adding MgO nanoparticles (25 mg) into 1 mL of DMSO solution with PUR (200 µM, Selleck, S3042, USA) and RA (200 µM, Solarbio, 302 794, China). Next, the mixture was placed in a constant shaker at 100 rpm and 37 °C for 24 h, then centrifuged at 5000 rpm for 20 min. After this step, the DMSO was removed, and the remaining MgO was washed with distilled water three times and then dried at 37 °C. A spectrophotometer (ThermoFisher, NanoDrop2000, USA) was used to measure the absorption peaks of the remaining DMSO at a wavelength of between 320 and 350 nm to calculate the concentration of PUR and RA, respectively. The doses of loaded drugs were calculated by the residual concentration.

Preparation of MgO/PLCL Scaffolds via Electrospinning: The MgO nanoparticles were mixed with PLCL (50:50, Daigang, Jinan, China) at weight ratios of 0:100, 10:100, 25:100, 50:100, and then dissolved in hexafluoroisopropanol (HFIP) (Aladdin, H10751, China) with the PLCL:HFIP ratio at 10% (w/v). The mixture was homogenized ultrasonically for 30 min and fully dissolved by magnetic stirring at room temperature. The MgO/PLCL solution was placed in a 5 mL syringe and pumped out through a 22G needle tip at a jet speed of 1.0 mL h^{-1}. Direct current with a voltage of 12 kV was applied, with a positive electrode connected to the needle tip and the ground wire connected to a pair of parallel metal rods 15 cm away from the needle. After the current was turned on, uniform and parallel microfibers were formed between metal rods. The microfibers were collected repeatedly with glass slides or 12 mm cell slides to form an aligned fiber membrane used for in vitro experiments. The MgO nanoparticles loaded with PUR and RA were used to fabricate PUR/RA-loaded MgO/PLCL scaffold.

Physical Characterizations of the MgO/PLCL Scaffolds: The microstructure of the scaffolds was imaged via scanning electron microscope (SEM) (Hitachi, S4800, Japan) and TEM. All samples were sputter-coated with gold for 60 s in the coating device (Quorum Technologies, SC7620, UK) and then observed under SEM at a voltage of 10 kV. The diameter of scaffold fibers was quantified via ImageJ (USA) based on the SEM images.

The hydrophilicity of the MgO/PLCL scaffolds at different ratios was characterized via a Drop Shape Analyzer (Krüss, DSA25, Germany) by measuring the contact angle after 30 s of a water drop on the scaffold surface.

The mechanical properties of scaffolds were measured using a universal testing machine (Shanghai Precision Instrument, HY10000, China). The MgO/PLCL (ratio of 0:100, 10:100, 25:100, 50:100) samples were molded into a strip with an original length of 100 mm and a width of 10 mm. The thickness of samples was measured via SEM. During tests, the samples were subjected to a constant tensile strain rate mode at 50 mm min^{-1}. The stress-strain curves were recorded for each group of scaffolds, and Young's modulus was calculated.

The Mg^{2+} Release Characteristics of MgO/PLCL Scaffolds: The Mg^{2+} release property was measured via a commercial kit (Solarbio, BC2795, China) after immersing samples in phosphate-buffered saline (PBS) for the indicated time. The cumulative Mg^{2+} release was calculated as follow:

$$E_r = \frac{V_e \sum_1^{n-1} C_i + V_0 C_n}{m} \quad (1)$$

E_r is the Cumulative release of ions, V_e is the volume of replaced buffer every time, V_0 is the total volume of buffer, C_i is the ion concentration at the *i*-th replacement, *m* is the total amount of ions in fiber membrane, *n* is the times of buffer replacement

The Responses of MgO/PLCL Scaffolds to the Acidic Environment: A cell culture medium (pH 6.5) simulated the acidic cerebrospinal fluid environment after SCI. The PLCL and MgO/PLCL (25:100) scaffolds fabricated on 12 mm cell slides were immersed in the medium (pH 6.5), and the pH value was detected every minute via pH meter (Leici, PHS3C, China).

Cell Culture: Isolation and culture of mouse bone marrow mesenchymal stromal cells (BMSCs) on MgO/PLCL scaffolds: The MgO/PLCL (0:100, 10:100, 25:100, 50:100) scaffolds were disinfected with 75% ethanol and ultraviolet radiation. Mouse BMSCs were isolated from 4-week-old ICR mice using a method provided by Huang et al.[36] BMSCs were cultured and passaged to P3, then seeded on the MgO/PLCL scaffolds at a density of 25 000 cells cm^{-2} in 24 well plates and cultured for 3 days. The cytoskeleton was observed via fluorescence microscope (Carl Zeiss, AX10, Germany) after being stained with Phalloidin-Alexa Fluor 488 (Beyotime, C2201S, China) and Hoechst 33 342 (Beyotime, C1022, China). Cell spreading area was quantified using ImageJ 2.3 (USA) based on three images for each group.

Isolation and culture of mouse neural stem cells (NSCs): The NSCs were isolated from the fetus of a pregnant E14 mouse. Briefly, the brain was isolated from a fetal mouse and was rinsed and immersed in PBS at 4 °C. Then the meningeal layer containing vessels was carefully stripped, and the anterior-middle 1/3 of the brain, including the subventricular zone and the subgranular layer of the dentate gyrus of the hippocampus, was isolated and digested with 0.125% Trypsin-EDTA (Gibco, 25200-056, USA) at 37 °C for 5 min to obtain NSCs. The NSCs were cultured in a complete NSC culture medium containing DMEM/F12 medium (Biosharp, BL305A, China), B27 supplement (2%, Gibco, 17 504 044, USA), EGF (20 ng mL^{-1}, PeproTech, 31 509, UK), and bFGF (20 ng mL^{-1}, PeproTech, 45 033, UK) in 24-well plates at a density of 100 000 cells cm^{-2}. The formation of neurospheres was observed after about 3 to 5 days of culture, and then the cells were passaged for further use. The NSCs were identified through immunofluorescence staining of Nestin (1:250, Sigma, MAB353, USA) and Sox2 (1:250, CST, 23 064, USA).

Isolation and culture of mouse cortical neurons: The procedures were similar to isolating NSCs, except that the cerebral cortex of fetal mouse was isolated. The cortical neurons were cultured in a neuronal culture medium containing Neurobasal medium (Gibco, 21 103 049, USA), B27 supplement (2%), and GlutaMAX supplement (1%, Gibco, 35 050 061, USA) in 24-well plates at a density of 20 000 cells cm^{-2}.

NSCs proliferation assay: Mouse NSCs were seeded on various scaffolds (PLCL, MgO/PLCL, MgO/PLCL+PUR/RA) coated with Poly-D-lysine hydrobromide (PDL) (Sigma, P6407, USA) and Laminin (Gibco, 23 017 015, USA) in 24-well plates at a density of 20 000 cells cm^{-2} to measure proliferation via commercial EdU kit (Beyotime, C0071S, China) and CCK-8 kit (Beyotime, C0038, China). The EdU-labeled samples were co-stained with Nestin (1:250, Sigma, MAB353, USA).

Neuron protection in the acidic environment: The neuron culture medium was adjusted to pH 6.5 to mimic the acidic environment of SCI.[15] Mouse cortical neurons were seeded on 12 mm slides coated with PDL and Laminin in 24-well plates at a density of 20 000 cells cm^{-2} with normal culture medium for 3 days, then the medium was changed to pH 6.5, and a 0.5 cm×0.5 cm scaffold membrane (PLCL, MgO/PLCL, MgO/PLCL+PUR/RA) was also added. After 48 h of coculture, the cell viability was evaluated via a live/dead cell staining kit (Keygen Biotech, KGAF001, China). Lastly, quantitative analysis was performed by counting the percentage of live cells on three images in each group.

Neuron protection in NMDA-induced cytotoxic environments: The neuron culture medium with NMDA (50 µM, Selleck, S7072, USA) was prepared to simulate the cytotoxic environment of SCI.[16] Cortical neurons were seeded on scaffold membranes (PLCL, MgO/PLCL, MgO/PLCL+PUR/RA) in 24-well plates at a density of 20000 cells cm^{-2} with normal culture for 9 days, then replaced with medium with NMDA and cultured for another 24 h. Cell apoptosis was evaluated via immunofluorescence staining of CASP3 (1:400, Sigma, AB3623, USA) and Tuj1 (1:1000, Biolegend, 801 202, USA). The quantitative analysis was performed by counting the $CASP3^+$ cells on three images in each group.

Detection of neuronal Ca^{2+} influx induced by NMDA: Cortical neurons were seeded in 24-well plates at a density of 20 000 cells cm^{-2} with normal culture medium for 9 days, then replaced with medium with NMDA (50 µM), and the 0.5 cm×0.5 cm scaffold membrane (PLCL, MgO/PLCL) was also added in for a 24 h coculture. Then the cells were rinsed with PBS and incubated with Fluo-4 AM (4 µM, Beyotime, S1060, China) for 45 min, replaced with normal medium for another 30 min, and observed via a fluorescence microscope. The cellular Ca^{2+} concentration was proportional to the fluorescence intensity. The percentage of Fluo-4 AM^+ cells in each group was analyzed.

NSCs differentiation on scaffolds: The scaffold membranes (PLCL, MgO/PLCL, and MgO/PLCL+PUR/RA) were fabricated on 12 mm cell slides and coated with PDL and Laminin. The NSCs at P1 generation were seeded on membranes in 24-well plates at a density of 20 000 cells cm^{-2} and cultured with neuronal differentiation medium containing Neurobasal medium, 2% B27 supplement, 1% GlutaMAX supplement, and cultured for 7 days. Then the cells were fixed and subjected to immunofluorescence staining with GFAP (1:1000, CST, 80 788, USA) and Tuj1 (1:1000, Biolegend, 801 202, USA). The images were taken via fluorescence microscope. The proportion of Tuj1-labeled neurons was analyzed using GraphPad Prism 7.0 (USA). The morphological characteristics of axons of neurons differentiated from NSCs (20 neurons from each group) were analyzed through Sholl's analysis using ImageJ 2 (USA).[37]

Immunofluorescence (IF) staining of cells: Cell samples were fixed with 4% paraformaldehyde (PFA) for 15 min, then blocked with 2% bovine serum albumin (BSA) for 1 h. Samples were then incubated with primary antibody for 2 h at room temperature, followed by species-specific fluorescent secondary antibody incubation for 1 h at room temperature. Nuclei were stained with Hoechst 33 342 for 15 min at room temperature. The images were taken via a fluorescence microscope.

Animal Experiments: Six-week-old ICR female mice (25 g ± 5 g) were used in animal experiments. All animals were provided by the Experimental Animal Center of Soochow University (Suzhou, China), and the experiments were approved by the Ethics Committee of the First Affiliated Hospital of Soochow University (2012).

Mouse spinal cord hemisection model and scaffolds implantation: The mice were anesthetized intraperitoneally (ketamine 100 mg kg^{-1}, xylazine 10 mg kg^{-1}). The back skin was shaven and disinfected by povidone-iodine. A 2 cm incision was made longitudinally on the back, and the paraspinal muscles were separated to expose the T9 lamina. The spinal cord was exposed after T9 laminectomy, and then a 1 mm long hemisection defect injury was performed on the left half of the spinal cord with a sharp lancet. The scaffold membrane (PLCL, MgO/PLCL+PUR/RA) was curled along the fiber direction, cut into 1 mm cylinders, and then implanted into the defect site. The control group was subjected to injury but received no implantation. The muscle and skin were sutured separately, then the mice were resuscitated in a 37 °C incubator and reared in clean cages at room temperature. Mice were free to access food and water, and the urine was squeezed out every day after the surgery until the urinary function recovered or they were sacrificed.

Forty mice underwent SCI surgery in each group. At 3 days and 4 weeks after the surgery, three mice from each group were sacrificed by euthanasia to harvest fresh spinal cord for RT-PCR. Throughout the whole study, the unexpected death in each group was less than 10 mice. The remaining mice were sacrificed at 2 weeks ($n = 10$) and 8 weeks ($14 \leq n < 24$) after surgery to obtain spinal cord samples for IF staining.

Behavioral assessment: The locomotion recovery of the left hind limb of the mouse was evaluated via the Basso Mouse Scale (BMS) scoring system[38] weekly after surgery ($n = 10$). The test was carried out in an open-field box of 50 cm × 40 cm. The mouse was adapted to the environment for 30 min, and the urine of each mouse was squeezed out before the test. The test time was 4 min, with video recorded.

Immunofluorescence (IF) staining of the spinal cord: The spinal cord samples were fixed with 4% PFA for 24 h, then dehydrated using 10%, 20%, and 30% sucrose solution sequentially. Then the samples were sliced with a thickness of 20 µm by cryomicrotome (Leica, CM3050S, Germany). The cryosectioned samples were immersed in sodium citrate buffer (10 mM sodium citrate, pH 6.0) for 30 min at 80 °C for antigen retrieval, then incubated with blocking buffer (0.01 mM PBS, 10% Fetal bovine serum, and 0.3% TritonX-100) for 1 h at room temperature. After that, the sections were incubated with the primary antibody at 4 °C overnight, then incubated with species-specific fluorescent secondary antibody (1:500) for 1 h at room temperature. Nuclei were stained with Hoechst 33 342 for 15 min at room temperature. Lastly, the sections were fixed with an anti-fade mounting medium. The images were taken via a fluorescence microscope. Primary antibodies included: Tuj1 (mouse mAb, 1:400, Biolegend, 801 202, USA), Tuj1 (rabbit mAb, 1:400, Sigma, T2200, USA), GFAP (1:400, CST, 80 788, USA), CS-56 (1:400, Sigma, C8035, USA), Nestin (1:250, Sigma, MAB353, USA), CD68 (1:400, CST, 97 778, USA), and CASP3 (1:200, Sigma, AB3623, USA). Secondary antibodies included: goat anti-mouse IgG (Alex 488, Invitrogen, A11001, USA), goat anti-mouse IgG (Alex 594, Invitrogen, A11005, USA), goat anti-rabbit IgG (Alex 488, Invitrogen, A11008, USA), and goat anti-rabbit IgG (Alex 594, Invitrogen, A11012, USA).

In vivo biosafety tests: Mouse blood was collected from the medial canthus vein at 1 day, 3 days, and 1, 2, 3, 4, 6, and 8 weeks after surgery. The blood was kept at 37 °C for 1 h, then at 4 °C overnight, centrifuged at 1000 rpm for 10 min, and then the serum was obtained. The serum Mg^{2+} was detected via a commercial kit (Solarbio, BC2795, China). The renal function was assessed via serum creatinine (Cre, ShengGong, D799853, China) concentration, and the liver function was assessed via alanine transaminase (ALT) (ShengGong, D799580, China) and aspartate transaminase (AST) (ShengGong, D799582, China) activity.

Real-time PCR (RT-PCR) of spinal cord tissues: The expression of acid-sensing ion channel (ASIC3) genes and alkaline sensing channel (PKD2L1) genes on the spinal cord were quantified via real-time polymerase chain reaction (RT-PCR). The reverse transcription of total RNA was performed via the RevertAid First Strand cDNA Synthesis Kit (ThermoFisher, K1622, USA), and the PCR reaction system was prepared with SYBR Green qPCR Master Mix (Bimake, B21202, USA) and primers. The primers are listed in **Table 1**.

Statistical Analysis: All quantified data were presented as mean ± standard deviation (SD). Statistical analysis was performed using Graph-

Table 1. Primers for quantitative real-time PCR.

Gene	Forward (5′-3′)	Reverse (5′-3′)
ASIC3	TTCACCTGTCTTGGCTCCTC	TGACTGGGGATGGGATTTCTAAG
PKD2L1	TACCTCAGCAGCGTCTGGAACA	CTGCATACGTGTCTGGCTGTTG
Actin	CATTGCTGACAGGATGCAGAAGG	TGCTGGAAGGTGGACAGTGAGG

ASIC3: acid sensing ion channel 3; PKD2L1: polycystic kidney disease-protein-2-like 1.

Pad Prism 7.0 software (USA). One-way or two-way ANOVA coupled with Tukey's multiple comparison test were used to evaluate differences between groups. Unpaired two-tailed *t*-test was used to compare two groups. A probability value $p < 0.05$ was considered statistically significant.

Supporting Information

Supporting Information is available from the Wiley Online Library or from the author.

Acknowledgements

J.X. and J.L. contributed equally to this work. This work was supported by the National Key Research and Development Program (No. 2016YFC1100203, 2020YFC1107402), Innovation and Entrepreneurship Program of Jiangsu Province, A Priority Academic Program Development of Jiangsu Higher Education Institutions.

Conflict of Interest

The authors declare no conflict of interest.

Data Availability Statement

The data that support the findings of this study are available from the corresponding author upon reasonable request.

Keywords

magnesium, neural morphogens, neuroprotection, spinal cord injury

Received: February 18, 2022
Revised: April 22, 2022
Published online: June 3, 2022

[1] S. L. James, A. Theadom, R. G. Ellenbogen, M. S. Bannick, W. Montjoy-Venning, L. R. Lucchesi, *Lancet Neurol.* **2019**, *18*, 56.
[2] M. G. Fehlings, L. A. Tetreault, J. R. Wilson, B. K. Kwon, A. S. Burns, A. R. Martin, G. Hawryluk, J. S. Harrop, *Global Spine J.* **2017**, *7*, 84S.
[3] C. S. Ahuja, J. R. Wilson, S. Nori, M. R. N. Kotter, C. Druschel, A. Curt, M. G. Fehlings, *Nat. Rev. Dis. Primers* **2017**, *3*, 17018.
[4] J. H. Badhiwala, C. S. Ahuja, M. G. Fehlings, *J. Neurosurg. Spine* **2018**, *30*, 1.
[5] M. V. Nikolaev, L. G. Magazanik, D. B. Tikhonov, *Neuropharmacology* **2012**, *62*, 2078.
[6] a) E. Bain, T. Bubner, P. Ashwood, E. Van Ryswyk, L. Simmonds, S. Reid, P. Middleton, C. A. Crowther, *BMC Pregnancy Childbirth* **2015**, *15*, 176; b) J. L. Saver, S. Starkman, M. Eckstein, S. J. Stratton, F. D. Pratt, S. Hamilton, R. Conwit, D. S. Liebeskind, G. Sung, I. Kramer, G. Moreau, R. Goldweber, N. Sanossian, F.-M. Investigators Coordinators, *N. Engl. J. Med.* **2015**, *372*, 528; c) A. E. Kirkland, G. L. Sarlo, K. F. Holton, *Nutrients* **2018**, *10*, 730.
[7] I. Cernak, V. J. Savic, J. Kotur, V. Prokic, M. Veljovic, D. Grbovic, *J. Neurotrauma* **2000**, *17*, 53.
[8] D. B. Wiseman, A. T. Dailey, D. Lundin, J. Zhou, A. Lipson, A. Falicov, C. I. Shaffrey, *J. Neurosurg. Spine* **2009**, *10*, 308.
[9] a) C. A. Gregoire, B. L. Goldenstein, E. M. Floriddia, F. Barnabe-Heider, K. J. Fernandes, *Glia* **2015**, *63*, 1469; b) M. Stenudd, H. Sabelstrom, J. Frisen, *JAMA Neurol* **2015**, *72*, 235.
[10] a) C. S. Ahuja, A. R. Martin, M. Fehlings, *F1000 Faculty Rev-1017* **2016**, 5; b) H. Sabelstrom, M. Stenudd, J. Frisen, *Exp. Neurol.* **2014**, *260*, 44.
[11] a) I. B. Wanner, M. A. Anderson, B. Song, J. Levine, A. Fernandez, Z. Gray-Thompson, Y. Ao, M. V. Sofroniew, *J. Neurosci.* **2013**, *33*, 12870; b) M. A. Anderson, J. E. Burda, Y. Ren, Y. Ao, T. M. O'Shea, R. Kawaguchi, G. Coppola, B. S. Khakh, T. J. Deming, M. V. Sofroniew, *Nature* **2016**, *532*, 195.
[12] V. Ribes, J. Briscoe, *Cold Spring Harbor Perspect. Biol.* **2009**, *1*, a002014.
[13] J. Chen, S. Y. Leong, M. Schachner, *Eur. J. Neurosci.* **2005**, *22*, 1895.
[14] S. I. Jeong, B. S. Kim, S. W. Kang, J. H. Kwon, Y. M. Lee, S. H. Kim, Y. H. Kim, *Biomaterials* **2004**, *25*, 5939.
[15] E. Jalalvand, B. Robertson, H. Tostivint, P. Low, P. Wallen, S. Grillner, *J. Neurosci.* **2018**, *38*, 7713.
[16] F. X. Soriano, S. Papadia, F. Hofmann, N. R. Hardingham, H. Bading, G. E. Hardingham, *J. Neurosci.* **2006**, *26*, 4509.
[17] A. P. Tran, P. M. Warren, J. Silver, *Physiol. Rev.* **2018**, *98*, 881.
[18] N. R. Temkin, G. D. Anderson, H. R. Winn, R. G. Ellenbogen, G. W. Britz, J. Schuster, T. Lucas, D. W. Newell, P. N. Mansfield, J. E. Machamer, J. Barber, S. S. Dikmen, *Lancet Neurol.* **2007**, *6*, 29.
[19] T. K. McIntosh, A. I. Faden, I. Yamakami, R. Vink, *J Neurotrauma* **1988**, *5*, 17.
[20] T. Westermaier, S. Zausinger, A. Baethmann, R. Schmid-Elsaesser, *Acta Neurochir.* **2005**, *147*, 525.
[21] a) I. Lingam, C. Meehan, A. Avdic-Belltheus, K. Martinello, M. Hristova, P. Kaynezhad, C. Bauer, I. Tachtsidis, X. Golay, N. J. Robertson, *Pediatr. Res.* **2019**, *86*, 699; b) T. Westermaier, C. Stetter, G. H. Vince, M. Pham, J. P. Tejon, J. Eriskat, E. Kunze, C. Matthies, R. I. Ernestus, L. Solymosi, K. Roosen, *Crit. Care Med.* **2010**, *38*, 1284.
[22] F. Streijger, J. H. Lee, N. Manouchehri, E. B. Okon, S. Tigchelaar, L. M. Anderson, G. A. Dekaban, D. A. Rudko, R. S. Menon, J. F. Iaci, D. C. Button, A. M. Vecchione, A. Konovalov, P. D. Sarmiere, C. Ung, A. O. Caggiano, B. K. Kwon, *J. Neurotrauma.* **2016**, *33*, 2202.
[23] B. K. Kwon, J. Roy, J. H. Lee, E. Okon, H. Zhang, J. C. Marx, M. S. Kindy, *J. Neurotrauma.* **2009**, *26*, 1379.
[24] Y. Lai, Y. Li, H. Cao, J. Long, X. Wang, L. Li, C. Li, Q. Jia, B. Teng, T. Tang, J. Peng, D. Eglin, M. Alini, D. W. Grijpma, G. Richards, L. Qin, *Biomaterials* **2019**, *197*, 207.
[25] N. P. Rijal, U. Adhikari, S. Khanal, D. Pai, J. Sankar, N. Bhattarai, *Mater. Sci. Eng., B* **2018**, *228*, 18.
[26] H. Shen, C. Fan, Z. You, Z. Xiao, Y. Zhao, J. Dai, *Adv. Funct. Mater. 32*, 2110628.
[27] C. S. Ahuja, S. Nori, L. Tetreault, J. Wilson, B. Kwon, J. Harrop, D. Choi, M. G. Fehlings, *Neurosurgery* **2017**, *80*, S9.
[28] G. D. Zeevalk, W. J. Nicklas, *J. Neurochem.* **1992**, *59*, 1211.
[29] C. V. Pfenninger, C. Steinhoff, F. Hertwig, U. A. Nuber, *Glia* **2011**, *59*, 68.
[30] a) M. Daynac, L. Tirou, H. Faure, M. A. Mouthon, L. R. Gauthier, H. Hahn, F. D. Boussin, M. Ruat, *Stem Cell Rep.* **2016**, *7*, 735; b) S.

Mishra, K. K. Kelly, N. L. Rumian, J. A. Siegenthaler, *Stem Cell Rep.* **2018**, *10*, 1705.
[31] S. Jacobs, D. C. Lie, K. L. DeCicco, Y. Shi, L. M. DeLuca, F. H. Gage, R. M. Evans, *Proc. Natl. Acad. Sci. U. S. A.* **2006**, *103*, 3902.
[32] R. A. Ihrie, J. K. Shah, C. C. Harwell, J. H. Levine, C. D. Guinto, M. Lezameta, A. R. Kriegstein, A. Alvarez-Buylla, *Neuron* **2011**, *71*, 250.
[33] N. Stifani, *Front. Cell. Neurosci.* **2014**, *8*, 293.
[34] S. Arber, R. M. Costa, *Science* **2018**, *360*, 1403.
[35] V. Hiremath, R. Shavi, J. Gil Seo, *J. Colloid Interface Sci.* **2017**, *498*, 55.
[36] S. Huang, L. Xu, Y. Sun, T. Wu, K. Wang, G. Li, *J Orthop. Transl.* **2015**, *3*, 26.
[37] T. A. Ferreira, A. V. Blackman, J. Oyrer, S. Jayabal, A. J. Chung, A. J. Watt, P. J. Sjostrom, D. J. van Meyel, *Nat. Methods* **2014**, *11*, 982.
[38] D. M. Basso, L. C. Fisher, A. J. Anderson, L. B. Jakeman, D. M. McTigue, P. G. Popovich, *J. Neurotrauma.* **2006**, *23*, 635.